JOURNAL OF GUIDANCE, CONTROL, AND DYNAMICS
Vol. 21, No. 2, March–April 1998

Simulation of a Controlled Airfoil with Jets

Brian G. Allan*
NASA Langley Research Center, Hampton, Virginia 23681
and
Maurice Holt† and Andrew Packard‡
University of California, Berkeley, Berkeley, California 94720

Numerical simulations of a two-dimensional airfoil, controlled by an applied moment in pitch and an airfoil controlled by jets, were investigated. These simulations couple the Reynolds-averaged Navier–Stokes equations and Euler's equations of rigid-body motion, along with an active control system. Controllers for both systems were designed to track altitude commands and were evaluated by simulating a closed-loop altitude step response using the coupled system. The airfoil controlled by a pitching moment used an optimal state feedback controller. A closed-loop simulation of the airfoil with an applied moment showed that the trajectories compared very well with quasisteady aerodynamic theory, providing a measure of validation. The airfoil with jets used a controller designed by robust control methods. A linear plant model for this system was identified using open-loop data generated by the nonlinear coupled system. A closed-loop simulation of the airfoil with jets showed good tracking of an altitude command. This simulation also showed oscillations in the control input as a result of dynamics not accounted for in the control design. This research work demonstrates how computational fluid dynamics, coupled with rigid-body dynamics, and a control law can be used to prototype control systems in problematic nonlinear flight regimes.

Nomenclature

C_L = lift coefficient
C_M = moment coefficient
c = chord length
I_{yy} = moment of inertia in pitch
k = reduced frequency, $\omega c/2U_\infty$
M_u = applied moment in pitch
M_∞ = freestream Mach number
m = mass
$\dot{m}$ = mass flow rate
$\dot{m}^*$ = nondimensional mass flow rate, $\dot{m}/(\rho_\infty U_\infty S_{\text{jet}})$
q = dynamic pressure
Re = Reynolds number
S = reference area
S_{jet} = jet nozzle reference area
t = time
U_∞ = freestream velocity
u = control input
V = total velocity
z = altitude
α = angle of attack
Δ = uncertainty block
θ = pitch attitude
ρ = density
ω = angular velocity
$(\dot{})$ = derivative with respect to time
$\| \|_\infty$ = $\mathcal{H}_\infty$ norm

Subscripts

q = partial derivative with respect to pitch rate
α = partial derivative with respect to angle of attack
$\dot{\alpha}$ = partial derivative with respect to rate of change of angle of attack

Presented as Paper 97-0100 at the AIAA 35th Aerospace Sciences Meeting, Reno, NV, Jan. 6–9, 1997; received April 23, 1997; revision received Aug. 25, 1997; accepted for publication Aug. 25, 1997. Copyright © 1997 by the authors. Published by the American Institute of Aeronautics and Astronautics, Inc., with permission.

*Staff Scientist, Institute for Computer Applications in Science and Engineering. Member AIAA.
†Emeritus Professor, Department of Mechanical Engineering. Fellow AIAA.
‡Professor, Department of Mechanical Engineering.

Introduction

IN nonlinear flight regimes, the interaction between fluids, body dynamics, and controls can critically affect the performance of an aircraft. By coupling these disciplines one can computationally investigate the problematic nonlinear portions of the flight envelope. However, simulation models that rely on empiricism or linearity assumptions may give misleading results when applied to nonlinear flight regimes. To capture the nonlinear nature of the flowfield, higher-ordered models need to be considered. In this investigation, the Reynolds-averaged Navier–Stokes (RANS) equations are coupled with Euler's equations of motion, along with an active control system.

The application that provides the impetus for this work is the controlled landing of a high-performance powered-lift aircraft. This flight regime is currently problematic due to the difficulties in obtaining an adequate representation of the stability derivatives. In turn, use of a poor plant description to design the control system can lead to the loss of aircraft and pilot. The results of this research would begin to provide a control system designer with a means of computationally testing the control system in problematic nonlinear flight regimes, thus helping to avoid these costly errors.

Previous efforts have validated the component problems of unsteady fluid dynamics,[1] the specified trajectory of a descending powered-lift aircraft,[2] and the coupled fluids/body dynamics problem.[3] The coupled fluid, dynamics, and controls problem has been previously investigated for a three-dimensional store separation problem.[4] The case demonstrated here uses a similar methodology to describe the fluid and body dynamics by using a diagonalized implementation of the RANS equations in an overset mesh framework and Euler's equations of motion to describe the rigid-body response to aerodynamic loads. This study is different from the store separation problem, as the interaction between fluid dynamics, rigid-body motion, and controls for the store problem was small. This was a result of the large ejection force on the missile, which dominated the trajectory of the store. Here, the interaction between fluids, rigid-body dynamics, and controls is much more complex. The problem explored will demonstrate the potential of coupling these disciplines for prototyping control systems in nonlinear flight regimes.

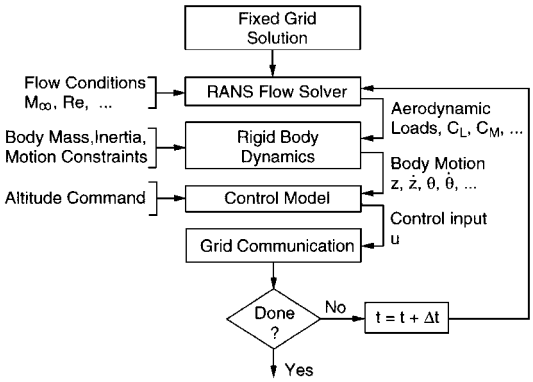

Fig. 1 Overall coupled system approach.

Approach

The coupling used to solve this problem is shown schematically in Fig. 1. This simulation starts with a converged fixed grid solution. The integrated aerodynamic loads and body states are passed from the flow solver to the six-degree-of-freedom, rigid-body dynamics code. The new body position is then integrated one time step given the mass, moment of inertia, and applied forces. Any kinematic constraints on the body are also applied to the body motion at this time. The new body state is then passed to the controls module, which generates a control input given the commanded altitude. Finally, the overlapped airfoil and jet grids are repositioned on the background mesh. This repositioning of the grids requires that the intergrid communication between the overlapped grids be reestablished. This entire process is repeated every time step until the simulation is complete.

Flow Solver

The flowfield is computed by solving the RANS equations using the diagonal scheme of Pulliam and Chaussee[5] in the grid framework of Steger et al.[6] The equations are integrated through Euler implicit time marching and second-order spatial differencing with viscous wall conditions specified as no-slip, zero normal pressure gradient, and adiabatic. Information transferred between overset mesh boundaries is implemented using trilinear interpolation of the dependent variable vector, $\boldsymbol{Q} = [\rho, \rho u, \rho v, \rho w, e]^T$. The flow solver cost is 7 μs/cell/step using a single processor of a Cray C90. Turbulence was modeled using the algebraic model of Baldwin and Lomax[7] as implemented by Renze et al.[8]

Domain Decomposition

Computation of the loads generated by a dynamic vehicle requires accurate representation of the geometry and flowfield. For the cases shown in Figs. 2 and 3, the domain was discretized using a curvilinear airfoil and nozzle grids overset on a stretched Cartesian background mesh. Overlapped grid topologies of this type allow representation of complex geometries and movement of bodies without regeneration of component grids.[2,4,9] Because grid boundaries are not required to match neighboring grids, robust algebraic[10] and hyperbolic[11] grid generators can be used to obtain spacing and orthogonality control.

The exchange of flow information between the zones of an overlapping grid system is computed using a domain connectivity function. The donor–receiver relationship between the grids was established at each time step using an efficient search technique.[12] The relative cost of the intergrid communication to flow solver expense is dependent on the ratio of intergrid boundary points to volume points.

The overset mesh topology used for the airfoil with jets is shown in Figs. 2 and 3. Here, the intergrid boundaries comprise the outer boundary of the airfoil and nozzle grids, as well as the hole boundary in the background and airfoil grids. Along the hole boundary in the background grid, $\boldsymbol{Q}$ is trilinearly interpolated from the solution field of the airfoil grid. Similarly, the outer boundary points of the airfoil grid are interpolated from the dependent variable vector of the background grid. This exchange of information establishes the intergrid communication between the grid zones for steady or unsteady fixed grid problems. Note that the boundary surface points

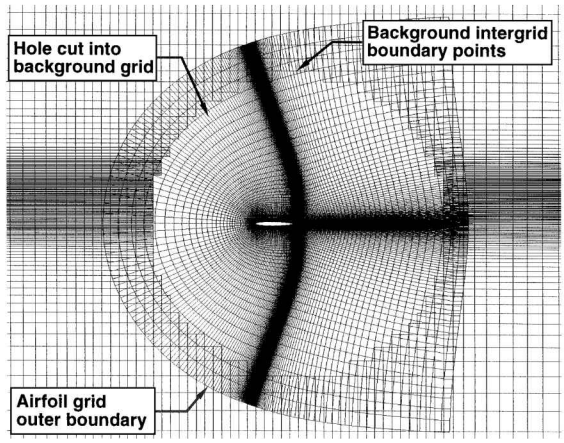

Fig. 2 Close-up view of the airfoil grid overset on a Cartesian background grid.

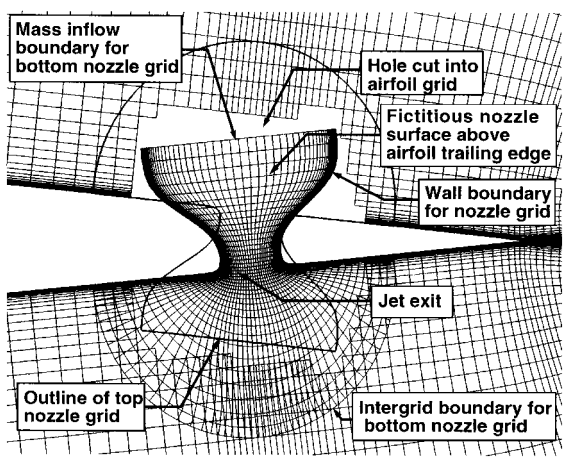

Fig. 3 Bottom nozzle grid at the trailing edge of the airfoil with an outline of the top nozzle grid.

of each implicit grid zone must be specified either by boundary conditions or through communication with other zones. For problems in which zones move relative to each other, as is the case for aerodynamically controlled vehicles, the intergrid communication must be reestablished at each time step.

Note that Fig. 3 shows the bottom nozzle grid at the trailing edge of the airfoil with an outline of the top nozzle grid. The upper part of the bottom nozzle grid, which extends above the airfoil surface, is fictitious and does not interact with the flowfield. These nozzle grids are used to allow the flow to develop as the mass flow rate is changed by the active controller at the inflow boundary.

Rigid-Body Dynamics

Rigid-body motion is described by a conservation of linear and angular momentum using coordinates fixed to the center of gravity of the body and aligned with its principal axes.[3] Euler parameters are used to describe the rotation of the body from its initial position. These parameters are integrated according to the rotational body dynamics, updated, and stored for each grid.[12,13] Kinematic constraints can be imposed during the trajectory for restricted degree-of-freedom simulations. In addition, the assumption of rigid-body dynamics eliminates the need to store the component grids for all time, inasmuch as the Euler parameters may be used to compute grid attitude from the initial position. Note that the timescales of fluid motion are typically many orders smaller than the rigid-body motion, making this loose coupling between the body motion and flow solver adequate.

Control Law

The airfoil controlled by an applied pitching moment used an optimal state feedback control law. Integral control was used to improve tracking performance of altitude commands. The altitude of the airfoil was controlled by adding an applied moment to the aerodynamic

Table 1 Quasisteady coefficients

C_{L_0}	0.00	C_{M_0}	0.00
C_{L_α}	6.28	C_{M_α}	0.00
C_{L_q}	1.44	C_{M_q}	−0.36
$C_{L_{\dot\alpha}}$	0.78	$C_{M_{\dot\alpha}}$	−0.35

forces, changing the attitude of the airfoil. This change in attitude produces aerodynamic lift, accelerating the airfoil vertically. The controller was designed using a linear time invariant system based on quasisteady aerodynamic theory. The feedback gains were then calculated using a linear quadratic regulator (LQR) method, resulting in optimal feedback gains for the linearized model.

In the second problem, the applied moment was replaced by two reaction control jets near the trailing edge. Because of the nonlinear nature of this system, a robust control design approach was used.[14] The linear plant model used in the control design was developed using input/output data generated by the coupled system. By using robust control design methods, a nominal linear model of the airfoil system can be parameterized by a measure of uncertainty. This parameterized uncertainty introduces unmodeled dynamics not accounted for by the nominal model. Therefore, by increasing the uncertainty in the model, the control design becomes increasingly robust to unmodeled dynamics not present in the linear nominal model.

Results

The coupled system methodology just described was applied to a two-dimensional airfoil with and without jets. Both systems had controllers designed to track altitude commands. The closed-loop response of the airfoil without jets, using the coupled system, was compared to a quasisteady aerodynamic model. The tracking performance of the airfoil with jets was evaluated from a closed-loop simulation of the coupled system.

Airfoil Controlled by Applied Moment

This system consists of a NACA 64A010 airfoil with an applied pitching moment added to the aerodynamic forces. The airfoil has two degrees of freedom, one in the vertical direction and the other in the pitch direction. A comparison of the closed-loop response of the coupled system was made by replacing the RANS equations with a quasisteady aerodynamic model. This comparison will provide some measure of validation for the coupled system.

Aerodynamic Model

The aerodynamic lift and moment coefficients for the airfoil are modeled using a quasisteady formulation.[15] These coefficients are expressed as

$$C_L(t) = C_{L_0} + C_{L_\alpha}\alpha(t) + C_{L_{\dot\alpha}}(l/V)\dot\alpha(t) + C_{L_q}(l/V)q(t)$$

$$C_M(t) = C_{M_0} + C_{M_\alpha}\alpha(t) + C_{M_{\dot\alpha}}(l/V)\dot\alpha(t) + C_{M_q}(l/V)q(t)$$

where C_L and C_M are the coefficients of lift and pitching moment about the quarter-chord location, respectively. The aerodynamic lift and moment in terms of C_L and C_M were

$$L(t) = C_L(t)\left(\tfrac{1}{2}\rho V^2 S\right), \qquad M(t) = C_M(t)\left(\tfrac{1}{2}\rho V^2 Sc\right)$$

The stability derivatives C_{L_α}, C_{L_q}, C_{M_α}, and C_{M_q} were evaluated from steady-state solutions of the RANS equations. The $C_{L_{\dot\alpha}}$ and $C_{M_{\dot\alpha}}$ stability derivatives were estimated from unsteady flow solutions of a plunging airfoil at a reduced frequency of $k = 0.7$. The terms C_{L_0} and C_{M_0} represent the lift and moment coefficients evaluated at $\alpha = \dot\alpha = q = 0$. All stability derivatives were evaluated for a freestream Mach number of 0.3, Reynolds number of 32×10^6, and a chord length of 4.6 m. The values calculated for the quasisteady model are given in Table 1.

Linearized Dynamic Model

The equation of motion used for the vertical direction, $m\ddot z = \sum F_z$, can be expressed as

$$m\ddot z(t) = L(t)\cos[\theta(t) - \alpha(t)] \tag{1}$$

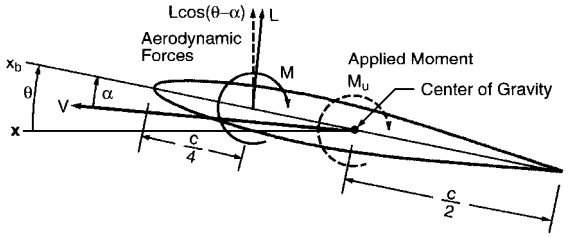

Fig. 4 Aerodynamic forces and notation.

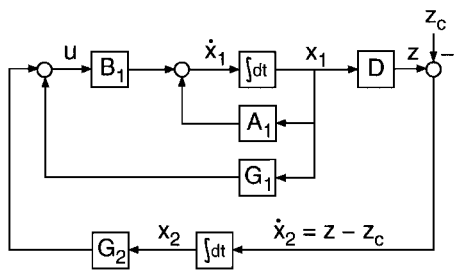

Fig. 5 Block diagram of the closed-loop system.

where gravitational and drag forces are neglected. Because the lift $L(t)$ is perpendicular to the total velocity of the airfoil (as shown in Fig. 4), it was multiplied by $\cos(\theta - \alpha)$ to obtain its vertical component.

The equation of motion in the pitch direction, $I_{yy}\ddot\theta = \sum M_y$, can be expressed as

$$I_{yy}\ddot\theta(t) = M(t) + L(t)\cos[\alpha(t)](c/4) + M_u(t) \tag{2}$$

where M_u was the applied pitching moment produced by the controller.

The quasisteady aerodynamic lift and moment equations were substituted into Eqs. (1) and (2) and linearized about the zero state. These equations were expressed as the linear time invariant system

$$\dot{\boldsymbol{x}}_1(t) = A_1\boldsymbol{x}_1(t) + B_1u(t) \tag{3}$$

where $\boldsymbol{x}_1 = [\theta, \dot\theta, z, \dot z]^T$. Numerical values for A_1 and B_1 were

$$A_1 = \begin{bmatrix} 0 & 1 & 0 & 0 \\ 3380 & 2.37 & 0 & -33.2 \\ 0 & 0 & 0 & 1 \\ 7780 & 123 & 0 & -76.2 \end{bmatrix}, \qquad B_1 = \begin{bmatrix} 0 \\ 2580 \\ 0 \\ 0 \end{bmatrix}$$

These matrices were calculated using $m = 62.8$ kg, $I_{yy} = 386$ kg·m^2, $M_\infty = 0.3$, and the coefficients in Table 1.

State Feedback Design

The state feedback controller used in this study incorporates integral control to improve tracking performance. Figure 5 shows a block diagram of the state feedback controller used. The objective of this control design is to find the optimal state feedback gains such that the altitude $z(t)$ tracks a commanded altitude path $z_c(t)$. Therefore, the error was defined as

$$e(t) = z(t) - z_c(t) = D\boldsymbol{x}_1(t) - z_c(t)$$

Using state and integral feedback, the input u was

$$u(t) = G_1\boldsymbol{x}_1(t) + G_2\int e(t)\,\mathrm{d}t$$

where G_1 and G_2 are the constant feedback gains. Now let $\dot{\boldsymbol{x}}_2(t) = e(t)$, where

$$\dot x_2(t) = D\boldsymbol{x}_1(t) - z_c(t) \tag{4}$$

Combining the linear systems from Eqs. (3) and (4) results in

$$\begin{bmatrix} \dot{\boldsymbol{x}}_1 \\ \dot x_2 \end{bmatrix} = \begin{bmatrix} A_1 & 0 \\ D & 0 \end{bmatrix}\begin{bmatrix} \boldsymbol{x}_1 \\ x_2 \end{bmatrix} + \begin{bmatrix} B_1 \\ 0 \end{bmatrix}u + \begin{bmatrix} 0 \\ -I \end{bmatrix}z_c$$

This can be expressed as one linear system:

$$\dot{\boldsymbol{x}}(t) = A\boldsymbol{x}(t) + Bu(t) + Fz_c(t)$$

where $\boldsymbol{x}(t) = [\boldsymbol{x}_1(t) \;\; x_2(t)]^T$. The input $u(t)$ for state feedback becomes

$$u(t) = \begin{bmatrix} G_1 \\ G_2 \end{bmatrix} \begin{bmatrix} \boldsymbol{x}_1(t) \\ x_2(t) \end{bmatrix} = G\boldsymbol{x}(t)$$

Optimal feedback gains were calculated by finding the input $u(t)$, which minimizes the quadratic integral cost function,

$$J(u(t)) = \int_0^\infty [\boldsymbol{x}^T(t)Q\boldsymbol{x}(t) + u^T(t)Ru(t)]\,\mathrm{d}t$$

where Q and R are positive-semidefinite symmetric matrices. The quantity $\boldsymbol{x}^T(t)Q\boldsymbol{x}(t)$ is a measure of how far the states deviate from the zero state at time t. The matrix Q is a diagonal weighting matrix where each diagonal element corresponds to a penalty on one of the states. The term $u^T(t)Ru(t)$ accounts for the amplitude of the input used to bring the system to the zero state. This optimal control design is known as the LQR problem.

The solution to this optimization problem is well known,[16] and it can be shown that the input that minimizes $J(u)$, given the system $\dot{\boldsymbol{x}}(t) = A\boldsymbol{x}(t) + Bu(t)$ and the initial condition $\boldsymbol{x}(0) = 0$, is

$$u_{\text{opt}}(t) = -R^{-1}B^T X\boldsymbol{x}(t)$$

Here, X is the solution to the algebraic Riccati equation

$$A^T X + XA - XBR^{-1}B^T X + Q = 0$$

where $A - BR^{-1}B^T X$ is stable. Thus, the optimal state feedback gains are

$$G = -R^{-1}B^T X$$

The optimal feedback gains G were calculated by first choosing initial values for the weights Q and R. After calculating the feedback gains G, the closed-loop response was simulated by solving Eqs. (1) and (2) coupled with the quasisteady aerodynamic model. These coupled equations were integrated in time using a fourth-order Runge–Kutta scheme. To assess the performance of the controller, a step in the commanded altitude of one chord length was simulated. The desired transient response for this simulation was a settling time of 1.0 s with minimum overshoot. If this performance criterion was not achieved, the weights were adjusted to increase or decrease the penalty of the individual states. This change in the weights resulted in an optimal controller with a new transient response. This cycle was iterated upon until the desired performance was achieved. The final iteration produced the feedback gains

$$G = [-193 \quad -13.1 \quad -2.43 \quad 1.07 \quad -3.00] \times 10^3$$

Airfoil with Applied Moment Simulation

A step command in altitude of one chord length from the starting position was simulated. Figure 6 shows states of the controlled simulation for the linear aerodynamic model and the nonlinear coupled system response. These two simulations match up very well, as would be expected in this linear flight regime. This comparison provides a measure of validation for the nonlinear coupled system. Instantaneous Mach contours of the simulation for the ascent of the airfoil to the reference altitude are shown in Fig. 7 at four different times.

In this simulation, the applied moment pitches the airfoil up, producing aerodynamic lift. This lift accelerates the airfoil in the vertical direction, moving the airfoil to the commanded altitude. As the airfoil starts to reach the commanded altitude, the controller produces a downward pitching moment. This applied moment pitches the airfoil down, which reduces the lift generated by the airfoil, slowing down its ascent. Figure 6 shows a small amount of overshoot of the commanded altitude, as predicted in the control design

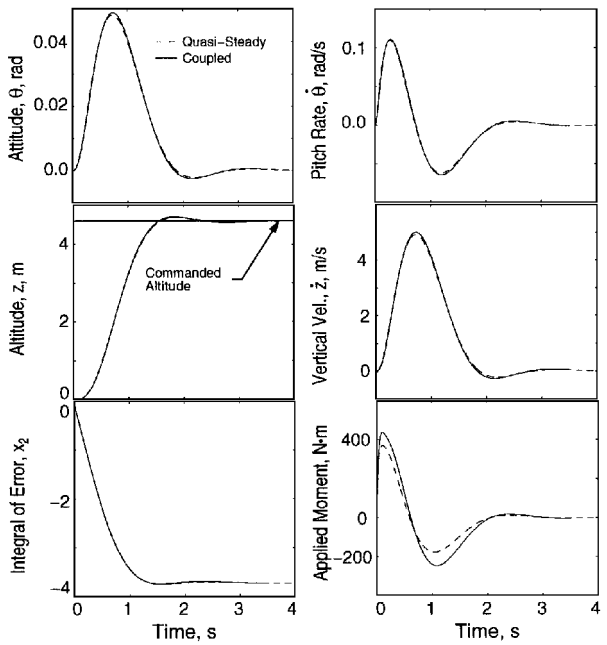

Fig. 6 Controlled response of the linear and coupled systems to a step input of 4.6 m in the commanded altitude.

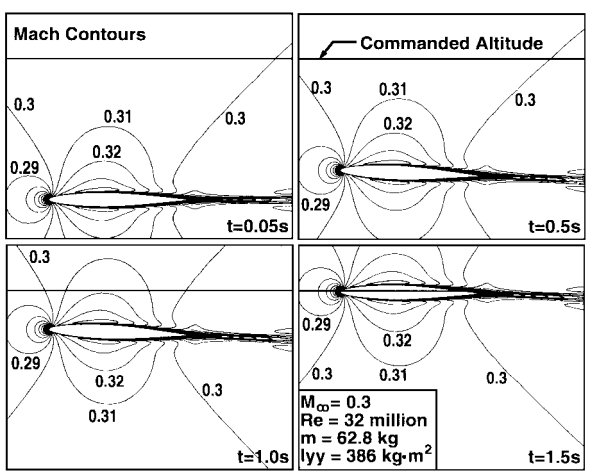

Fig. 7 Instantaneous Mach contours during the ascent of the airfoil to the commanded altitude.

using the quasisteady model. This overshoot was also seen in the RANS coupled simulation. A slight difference in the control moment generated can be seen in Fig. 6, where the quasisteady model predicts a smaller control input.

Airfoil Controlled by Jets

In this problem, the applied moment is replaced by two reaction control jets near the trailing edge of the airfoil. The center of gravity is placed at the quarter-chord location as shown in Fig. 8, increasing the stability of the system.

Note that the problem of resolving the complex flow of a two-dimensional jet in a crossflow was not addressed here because the purpose of this investigation was to demonstrate the analysis of a control system in a nonlinear flight regime. Therefore, an approximation to the jet flow was made by using coarse grids that do not resolve the complex flow associated with jets. However, it may be argued that the approximation made here is satisfactory for control design and analysis purposes as long as the flow being resolved captures the general dynamics of the system.

Plant Model Design

The highly nonlinear aerodynamic effects from the jets at the trailing edge of the airfoil make it very difficult to model. Figure 9

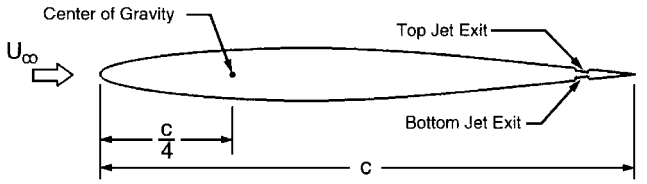

Fig. 8 Two-dimensional airfoil with jets problem.

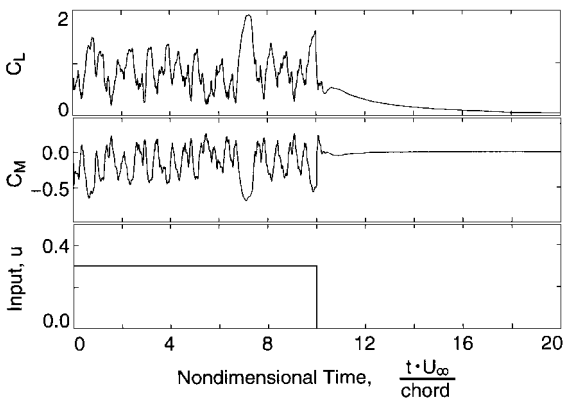

Fig. 9 Time histories of C_L and C_M for a fixed airfoil with the bottom jet turned on for a nondimensional mass flow rate of 0.3 from tU_∞/c = 0–10; time is nondimensionalized in terms of chord distances flown.

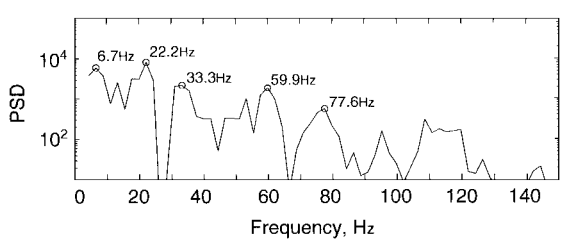

Fig. 10 Power spectral density of the C_L time history shown in Fig. 9 from tU_∞/c = 0–10, where U_∞ = 102 m/s and c = 4.6 m.

shows the aerodynamic lift and moment time histories for a fixed airfoil with a constant mass flow rate from the bottom jet. The aerodynamic forces have a large oscillatory behavior produced by the unsteady flow generated behind the jet. The large magnitude of these oscillations was due to the jet being two dimensional. The power spectral density of the C_L time history from $tU_\infty/c = 0$–10 is shown in Fig. 10. Figure 10 shows that the lift generated by a constant mass flow rate to the bottom jet does not have a dominant frequency. The approach used to model the dynamic response of the airfoil was to perform a system identification using input/output data. These input/output data were generated from two open-loop simulations using the coupled system. Note that a turbulence model was not used for this problem as it was not valid for this complicated unsteady flowfield.

The relationship between the input u and nondimensional mass flow rates to the top and bottom jets is shown in Fig. 11. A positive input u would correspond to a mass flow rate to the bottom jet and a negative u for the top jet, where u has a magnitude limit of 0.3.

The variables u_T and u_B are functions of the input u and are defined in the following way:

$$u_T = \begin{cases} 0 & u \le 0 \\ u & 0 < u \le 0.3, \\ 0.3 & 0.3 < u \end{cases} \qquad u_B = \begin{cases} 0.3 & u < -0.3 \\ -u & -0.3 \le u < 0 \\ 0 & 0 \le u \end{cases}$$

A delay for the mass flow rate command and the actual mass flow rate applied to the nozzles is modeled by $1/(\tau s + 1)$, as shown in Fig. 11, where $\tau = 4.5 \times 10^{-4}$.

The nondimensional mass flow rates $\dot{m}^*_{\text{top}}$ and $\dot{m}^*_{\text{bot}}$ were applied to the top and bottom nozzle grids, respectively. These mass flow rates were used to change the inflow boundary conditions on the nozzle

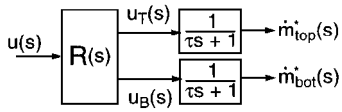

Fig. 11 Block diagram showing the relation between the input u and the nondimensional mass flow rates to the top and bottom jets in the Laplacian domain.

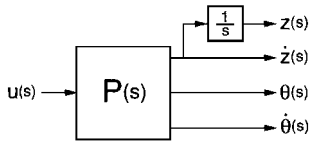

Fig. 12 State-space model with integrator and added $\dot{\theta}$ output.

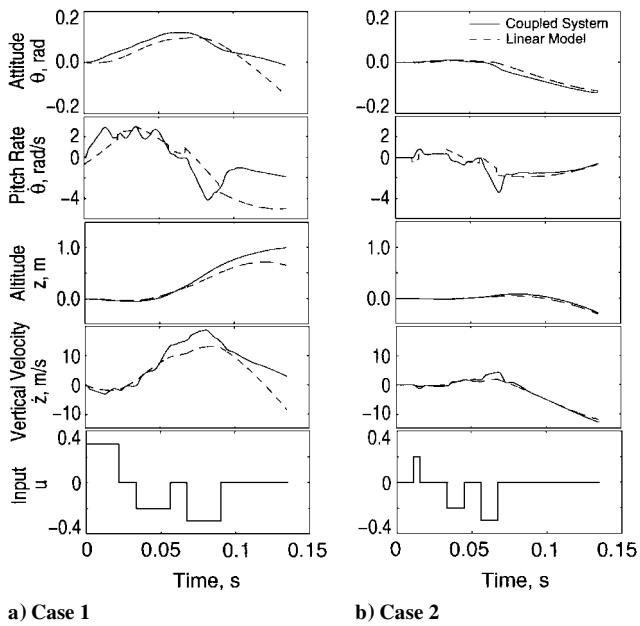

a) Case 1 **b) Case 2**

Fig. 13 Two open-loop simulations of the nonlinear coupled system with the linear input/output model response.

grids shown in Fig. 3. Note that a value of $\dot{m}^* = 0.1$ would correspond to a mass flow rate of $\dot{m} = 13.7$ kg/s at the inflow boundary.

The state-space model developed has an input u, with outputs $\dot{z}$ and θ. The altitude z was found by integrating $\dot{z}$. The pitch rate was produced by restructuring the linear system to obtain $\dot{\theta}$. This was done by first looking at the output equation

$$\boldsymbol{y} = \begin{bmatrix} \dot{z} \\ \theta \end{bmatrix} = \begin{bmatrix} c_1 \\ c_2 \end{bmatrix} \boldsymbol{x}$$

Thus the pitch rate could be expressed as

$$\dot{\theta} = c_2 \dot{\boldsymbol{x}} = c_2(A\boldsymbol{x} + Bu)$$

Restructuring the output equation to include $\dot{\theta}$ resulted in

$$\boldsymbol{y} = \begin{bmatrix} \dot{z} \\ \theta \\ \dot{\theta} \end{bmatrix} = \begin{bmatrix} c_1 \\ c_2 \\ c_2 A \end{bmatrix} \boldsymbol{x} + \begin{bmatrix} 0 \\ 0 \\ B \end{bmatrix} u$$

This system, $P(s)$, is shown in Fig. 12, where the altitude was found by integrating the vertical velocity.

The input u and states $\boldsymbol{x}$ for the open-loop simulations are shown in Fig. 13, where $u(t)$ was a series of step commands. The first simulation is shown in Fig. 13a, and the second in Fig. 13b. The model was identified using both sets of input/output data simultaneously. A comparison of the coupled simulation and linear model is shown in Fig. 13. This comparison shows how the simple two-state model captures the general behavior of the coupled system for the given inputs. The model compares relatively well for the second simulation

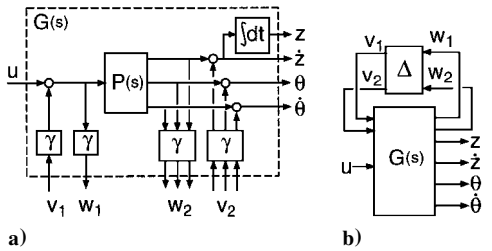

Fig. 14 Uncertainty model for $P(s)$: a) uncertainty block Δ not connected, where γ determines the amount of uncertainty; and b) plant $G(s)$ with full uncertainty block Δ.

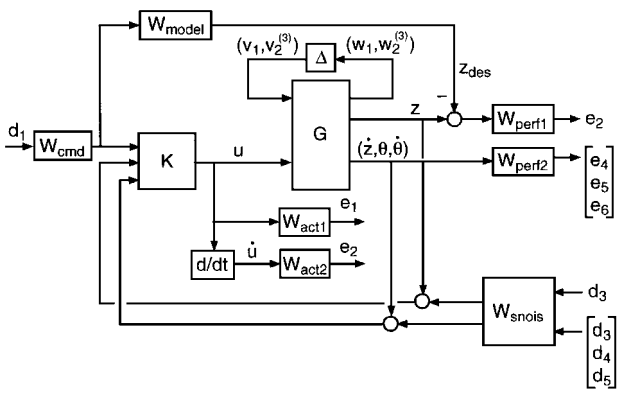

Fig. 15 Block diagram of performance weights for robust control design.

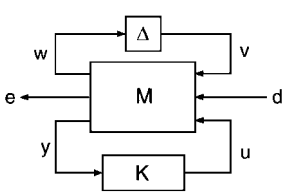

Fig. 16 Closed-loop system with performance weights and plant model G contained in M.

and for the beginning of the first simulation. In the first simulation, the model and coupled response start to diverge near $t = 0.1$ s. This could be a result of the larger attitude and pitch rate as compared with the second simulation.

Robust Control Design

The model used for the robust control design consists of the nominal model $P(s)$ and the elements γ and Δ, which parameterize the uncertainty in the model. This system is shown in Fig. 14, where γ is a scalar and determines the amount of uncertainty in the model. The transfer function Δ is assumed stable and unknown, except for the norm condition, $\|\Delta\|_\infty \leq 1$. The interconnection for the inputs w and outputs v to the Δ block are shown in Fig. 14a. The perturbed system with Δ connected is shown in Fig. 14b.

The block diagram in Fig. 15 shows the performance weights and disturbances used for the robust control design.[14] The W_{model} block was the ideal model response, which was represented by a well-damped, second-ordered system. The performance weight W_{cmd} defines the magnitude and frequency of the input commands to be tracked. W_{act1} and W_{act2} were penalty weights on the input u and its rate $\dot{u}$. The difference in the altitude and the ideal altitude response was weighted by W_{perf1}. The attitude, pitch rate, and vertical velocity were weighted by W_{perf2}. Noise was added to the system by inputs d_3–d_5 and shaped by W_{snois}, which set the magnitude and frequency range.

The performance weights and plant G in Fig. 15 were reduced to the block M shown in Fig. 16. The controller K was designed so that the perturbed system was stable and the transfer function from $\boldsymbol{d}$ to $\boldsymbol{e}$ satisfies

$$\|T_{\text{ed}}(M, K, \Delta)\|_\infty < 1$$

for all stable perturbations, Δ satisfying $\|\Delta\|_\infty \leq 1$.

The controller K was determined by using μ synthesis, which was approximated by an iterative method known as D–K iterations.[14] The original controller K, which had 68 states, was reduced to 17 states by performing a balanced realization.[17] This reduced controller was then used for the coupled RANS simulation.

Airfoil with Jets Simulation

The input $\boldsymbol{y}$ to the controller K was a vector containing the commanded altitude and the states, where $\boldsymbol{y} = [z_c, z, \dot{z}, \theta, \dot{\theta}]$. The controller takes these inputs and generates the signal $u(t)$, which is passed through the block shown in Fig. 11. This produces mass flow rates for the inflow boundary on the nozzle grids.

Performance of the controller was evaluated by analyzing the closed-loop response of the airfoil to a step input in the commanded altitude. Figure 17 shows the states for the simulations using the linear and nonlinear models. The altitude trajectory for the linear model was very good and was nearly identical to the ideal model response. The altitude trajectory for the coupled system was also good. It showed that the controller was able to track the desired altitude trajectory within the prescribed tracking performance.

The nonlinear simulation also revealed oscillations in the control jets not shown in the linear model simulation. The difference between these two simulations shows how the nonlinear dynamics were not captured by the linear plant model. These oscillations are induced by the controller, which is trying to force the nonlinear airfoil system to follow the desired altitude response of a linear system model W_{model}. The frequency of these oscillations is thought to be partly related to the altitude-tracking performance W_{perf1} used to design the controller. By increasing the tracking performance, the controller will try to keep the airfoil even closer to the desired altitude path, increasing the frequency of the oscillations.

The instantaneous Mach contours for the coupled simulation are shown in Fig. 18 at four different times. Figure 18 reveals the

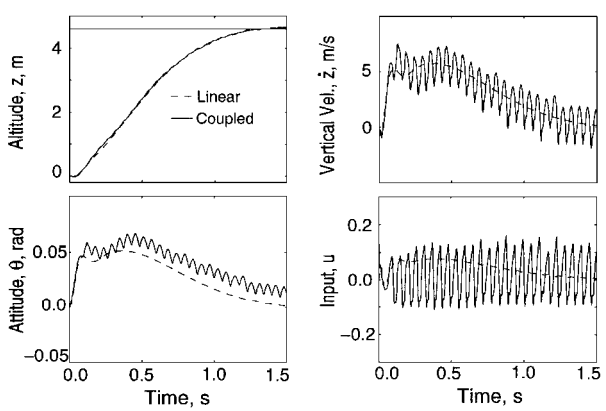

Fig. 17 Comparison of the states for the linear and coupled simulations.

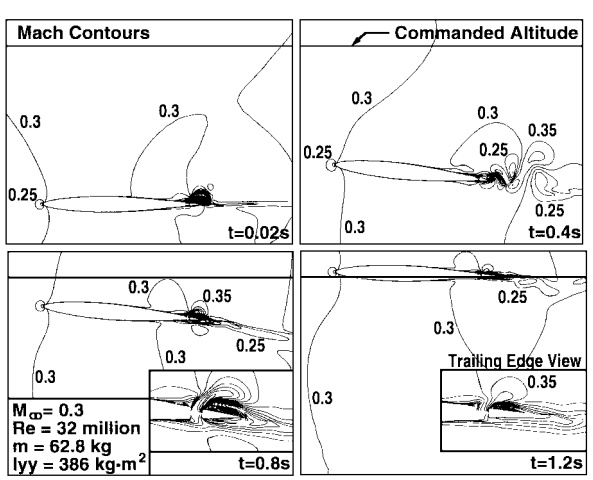

Fig. 18 Instantaneous Mach contours during the ascent of the airfoil to the commanded altitude.

complicated flow pattern generated by the top and bottom jets during the closed-loop simulation. The instantaneous Mach contours at $t = 0.02$ s show the flowfield just after the top jet was turned on by the controller. This top jet produces aerodynamic forces pitching the airfoil up. As the airfoil pitches up, aerodynamic lift is generated and begins to move the airfoil vertically. The instantaneous Mach contours at $t = 0.4$ s show the unsteady wake behind the airfoil as a result of the oscillations in the top and bottom jets. A close-up view of the trailing edge can be seen in the last two parts of Fig. 18. This view shows the unsteady flow behind the top jet where a low-pressure region has developed. At $t = 1.2$ s the airfoil has reached the commanded altitude.

Conclusions

The analysis of an aircraft control system for nonlinear flight regimes is complicated by the interaction of fluid dynamics, rigid-body dynamics, and the control system itself. Of particular interest is the landing of a powered-lift aircraft that has a strong interaction between the lifting jets and ground plane. Toward the goal of analyzing this system, the coupling of the RANS equations and Euler's equations of rigid-body motion with an active control system was performed. As a demonstration problem, the altitude control of airfoils with and without jets was investigated.

The airfoil without jets was controlled by an applied moment and used an optimal state feedback controller with integral control. The control design used an LQR method with a linear time invariant system based on quasisteady aerodynamics. The stability derivatives for this model were computed using steady and unsteady solutions to the RANS equations. A step in the commanded altitude was simulated by the RANS coupled system, which compared well with the quasisteady model. This comparison provided a measure of validation for the nonlinear coupled system.

The airfoil controlled by jets used a robust control design method. The linear plant model, used in the control design, was developed by performing a system identification on the input/output data. These input/output data were generated by two open-loop simulations of the coupled system. Simulation of the closed-loop response of the airfoil with the coupled system demonstrated that the airfoil was able to track the desired altitude trajectory within the specified performance. It also showed oscillations in the control jets that were not predicted by the linear model simulation.

Acknowledgments

This investigation was supported by the NASA Graduate Student Researchers Program in High Performance Computing and Communication, Fellowship NGT-51030 and by NASA Ames Consortium NCA2-782 and NCC2-5035. This research was also partially supported under NASA Contract NAS1-19480 while the first author was in residence at the Institute for Computer Applications in Science and Engineering (ICASE), NASA Langley Research Center, Hampton, Virginia. Computations were performed on the Numerical Aerodynamic Simulation facility Cray C90 and workstations at the Computational Aerosciences Branch and ICASE. Special thanks are owed to Chris Atwood for his assistance with problem development, software tools, and interpretation of results.

References

[1] Atwood, C. A., and Van Dalsem, W. R., "Flowfield Simulation About the SOFIA Airborne Observatory," *Journal of Aircraft,* Vol. 30, No. 5, 1993, pp. 719–727.

[2] Chawla, K., and Van Dalsem, W. R., "Numerical Simulation of STOL Operations Using Thrust-Vectoring," AIAA Paper 92-4254, Aug. 1992.

[3] Meakin, R. L., and Suhs, N., "Unsteady Aerodynamic Simulation of Multiple Bodies in Relative Motion," AIAA Paper 89-1996, June 1989.

[4] Atwood, C. A.,"Computation of a Controlled Store Separation from a Cavity," *Journal of Aircraft,* Vol. 32, No. 4, 1995, pp. 846–852; also AIAA Paper 94-0031, Jan. 1994.

[5] Pulliam, T. H., and Chaussee, D. S., "A Diagonal Form of an Implicit Approximate-Factorization Algorithm," *Journal of Computational Physics,* Vol. 39, Feb. 1981, pp. 347–363.

[6] Steger, J. L., Dougherty, F. C., and Benek, J. A., "A Chimera Grid Scheme," *Advances in Grid Generation,* edited by K. N. Ghia and U. Ghia, ASME FED-Vol. 5, American Society of Mechanical Engineers, New York, 1993, pp. 59–69.

[7] Baldwin, B. S., and Lomax, H., "Thin-Layer Approximation and Algebraic Model for Separated Turbulent Flows," AIAA Paper 78-257, Jan. 1978.

[8] Renze, K., Buning, P., and Rajagoplan, R., "A Comparative Study of Turbulence Models for Overset Grids," AIAA Paper 92-0437, Jan. 1992.

[9] Meakin, R. L., "Moving Body Overset Grid Methods for Complete Aircraft Tiltrotor Simulations," AIAA Paper 93-3350, July 1993.

[10] Steinbrenner, J. P., Chawner, J. R., and Fouts, C. L., "A Structured Approach to Interactive Multiple Block Grid Generation," *Applications of Mesh Generation to Complex 3-D Configurations,* AGARD-CP-464, 1989, pp. 8.1–8.12.

[11] Chan, W. M., and Steger, J. L., "Enhancements of a Three-Dimensional Hyperbolic Grid Generation Scheme," *Applied Mathematics and Computation,* Vol. 51, Oct. 1992, pp. 181–205.

[12] Meakin, R. L., "A New Method for Establishing Inter-Grid Communication Among Systems of Overset Grids," AIAA Paper 91-1586, June 1991.

[13] Meakin, R. L.,"Computations of the Unsteady Flow About a Generic Wing/Pylon/Finned Store Configuration," AIAA Paper 92-4568, Aug. 1992.

[14] Packard, A., Doyle, J., and Balas, G., "Linear, Multivariable Robust Control with a μ Perspective," *Journal of Dynamic Systems, Measurement and Control,* Vol. 155, June 1993, pp. 426–437.

[15] Tobak, M., and Schiff, L. B., "Aerodynamic Mathematical Modeling—Basic Concepts," *Dynamic Stability Parameters*, AGARD-LS-114, 1981, pp. 1.1–1.32.

[16] Kwakernaak, H., and Sivan, R., *Linear Optimal Control Systems,* Wiley, New York, 1972, pp. 193–248.

[17] Glover, K., "All Optimal Hankel-Norm Approximations of Linear Multivariable Systems and Their L_∞ Error Bounds," *International Journal of Control,* Vol. 39, No. 6, 1984, pp. 1115–1193.